AIAA JOURNAL
Vol. 40, No. 7, July 2002

Nodal Temperature Estimation Algorithms for Nonlinear Thermal Network Models

Miltiadis V. Papalexandris,* Mark H. Milman,† and Marie B. Levine†
Jet Propulsion Laboratory, California Institute of Technology, Pasadena, California 91109

Algorithms for estimating temperatures at arbitrary nodes of steady-state thermal network models, given noisy measured values of a subset of the nodes of the network, are described. Applications where temperature estimation is desired include correlation of test and analysis results, thermal-stress estimation, and others. An optimization problem is formulated to recover the temperatures at the unobservable nodes. This problem is an example of nonlinear, least-squares minimization with a single quadratic constraint (imposed by the measured data) and is solved with the method of Lagrange multipliers. New algorithms are developed that find local minima of the cost functional through a Newton-type iteration procedure. At each iteration a least-squares problem with a quadratic inequality is solved with a fast and memory-efficient method. The proposed algorithms are shown to be at least an order of magnitude faster than standard algorithms. Their accuracy and speed are examined through a series of tests on thermal models from ongoing NASA missions.

I. Introduction

PHYSICAL and economic constraints typically limit the number of temperature sensors that can be used on a thermal test of a system. These limitations include laboratory or field restrictions, available number of data channels, inaccessibility of certain parts of the system, etc. However, it is often desired to have temperatures of the system at more locations than those allowed by these constraints. Common reasons include correlation of test and analysis results at all nodes represented in the full thermal model of the system, estimation of thermal stresses, temperature node visualization, and others. Our particular motivation for developing temperature estimation methodologies stems from an ever-increasing demand for highly accurate thermal analysis and simulation of spacecraft. These demands are particularly challenging for several planned spaceborne science instruments, such as the Next Generation Space Telescope[1] and the Space Interferometry Mission.[2] The objective of this work is to develop methodologies that combine a priori models with measured temperature data to improve the accuracy of the estimate of the global temperature distribution obtained from the model alone.

Although analytical models are commonly developed to assess the global temperature profile of the system, discrepancies often arise between the mathematical predictions and the actual temperatures obtained through experimental data. Errors are typically due to modeling uncertainties (for example, physical properties of materials, model resolution, and connectivities), experimental measurement errors, or errors in the assumed input heat load. The intent here is to develop a methodology that would improve the model's predictive accuracy of the global temperature profile by using measured test data at selected measurement nodes in conjunction with the analytical model. The analogous problem of predicting global mechanical motions from a reduced set of measurement nodes through structural models has been studied extensively over the years; for example, see Guyan,[3] Kidder,[4] Levine et al.,[5] Kammer,[6] Smith and Beattie,[7] and Zimmerman and Kaouk.[8] Although significant work has appeared in related areas such as parameter identification and inverse problems for thermal systems (e.g., Beck et al.,[9] Alifanov,[10] Hensel,[11] Kurpisz and Nowak[12] and references therein), techniques for predicting global system temperatures from a limited set of measured temperatures has not seen a similar development.

The methods that have been developed for structural problems are restricted to linear models and, thus, are not directly transferable to thermal network problems in which radiation contributes significantly to heat exchange in the system. The challenge presented by these nonlinear network models is twofold. The first is to formulate a tractable mathematical problem that captures the high-level objective of improving the predictive accuracy of the analytical model by incorporating measured data. Second, because of the inherent nonlinearities in these problems and the ever increasing size of the thermal networks of interest, a concomitant challenge arises to develop robust and fast numerical methods to solve the resulting problem.

The general approach we settle on is to determine the global temperature set that minimizes the energy imbalance of the analytical model while meeting the accuracy constraints imposed at the measured nodes. Section II contains a discussion of various mathematical instantiations of this approach. The optimization problem that emerges from these considerations is a nonlinear least-squares problem with a scalar quadratic inequality constraint. Two different strategies (leading to two different minimization problems) are proposed and analyzed. A standard technique for nonlinear programming, the sequential quadratic programming (SQP) method is first examined. This proves to be very slow for large-scale problems. Subsequently, new algorithms are proposed with improved speed that take advantage of the particular structure of the network equations, as has been previously exploited by Milman and Petrick[13] and Papalexandris and Milman.[14] These algorithms belong to the class of Gauss–Newton iterative methods. Each iteration involves solving a least-squares problem with a single quadratic constraint (LSQI).[15] Traditional techniques for the LSQI problem[15] employ singular value decomposition, which becomes prohibitively slow for large problems. Again, by exploitation of the problem structure, a new method for the LSQI problem is developed that relies on the much faster QR decomposition.[15] This new algorithm also leverages on the problem feature that the observed nodes comprise a small subset of the total degrees of freedom of the system, thus leading to a significant computational savings in solving each linear subproblem.

This paper is divided as follows: Section II contains a brief description of the thermal network equations and the formulation of the node-prediction problem. Sections III and IV describe briefly the SQP method and in detail the proposed algorithms for solving the problems of interest. In Sec. V, the efficacy of the proposed algorithms is examined through numerical tests on large-scale spacecraft models that have been used in ongoing NASA projects.

Received 12 February 2001; revision received 21 December 2001; accepted for publication 28 December 2001.

*Member of the Staff. Member AIAA.
†Principal Member of the Staff.

II. Formulation of the Temperature Estimation Problem

This section is devoted to a brief description of the thermal network equations and the formulation of the temperature estimation problem. The following definitions are necessary for the discussion that follows. Let $\mathbb{R}^N$ be the real, N-dimensional linear space of column vectors $\boldsymbol{x} = [\boldsymbol{x}_1, \ldots, \boldsymbol{x}_N]^T$. The coordinatewise partial ordering on $\mathbb{R}^N$ implies that if $\boldsymbol{x}, y \in \mathbb{R}^N$, then $\boldsymbol{x} \geq y$ if and only if $\boldsymbol{x}_i \geq y_i$ for all $i = 1, \ldots, N$. The Euclidean norm

$$|\boldsymbol{x}| = \left\{ \sum_{i=1}^{N} x_i^2 \right\}^{\frac{1}{2}}$$

in $\mathbb{R}^N$ will also be used. Finally, let $\mathbb{R}_+^N = \{x \in \mathbb{R}^N : x \geq 0\}$.

A thermal network is defined as a set of nodes that are connected to each other via linear or quartic conductances.[16] In principle, it arises from a finite difference discretization of the heat transfer equation. Often, however, the network approach is adopted to construct models of complex systems in which a node is merely an isothermal component of the system.

In general, a thermal network model consists of N interior nodes and n boundary nodes. The steady-state temperature distribution on the interior nodes $[\boldsymbol{T}_1, \ldots, T_N]$ satisfies the following system of N nonlinear algebraic equations:

$$\hat{Q}_i + \sum_{j=1}^{N+n} \hat{C}_{ij}(\boldsymbol{T}_j - T_i) + \sum_{j=1}^{N+n} \hat{R}_{ij}\left(T_j^4 - \boldsymbol{T}_i^4\right) = 0 \qquad i = 1, \ldots, N \quad (1)$$

In Eqs. (1), $\hat{Q}_i$ are the external heat loads on the system, and $\hat{C}_{ij}$ and $\hat{R}_{ij}$ are the conduction and radiation coefficients of the system, respectively. The temperature distribution $\boldsymbol{T}_{N+1}, \ldots, T_{N+n}$ on the boundary nodes is assumed to be known and given.

The network system can be written in a matrix form after the following substitutions. First, let $\boldsymbol{T} = [\boldsymbol{T}_1, \ldots, T_N]^T$, $D(\boldsymbol{T}) = [T_1^4, \ldots, \boldsymbol{T}_N^4]^T$, and $D'(\boldsymbol{T}) = [\boldsymbol{T}_1^3, \ldots, T_N^3]^T$. Further, define the $N \times N$ matrices C and R as

$$C_{ij} = \begin{cases} \hat{C}_{ij}, & \text{if} \quad i \neq j \\ -\sum_{j=1}^{N+n} \hat{C}_{ij}, & \text{if} \quad i = j \end{cases} \quad (2)$$

$$R_{ij} = \begin{cases} \hat{R}_{ij}, & \text{if} \quad i \neq j \\ -\sum_{j=1}^{N+n} \hat{R}_{ij}, & \text{if} \quad i = j \end{cases} \quad (3)$$

Finally, let $\boldsymbol{Q} = [\boldsymbol{Q}_1, \ldots, Q_N]^T$ be the forcing vector of system (1), arising from the combination of the heat loads $\hat{\boldsymbol{Q}}_i$ and the energy exchange through the boundary nodes, that is,

$$Q_i = \hat{\boldsymbol{Q}}_i + \check{\boldsymbol{Q}}_i, \qquad i = 1, \ldots, N \quad (4)$$

with

$$\check{Q}_i = \sum_{j=N+1}^{N+n} \hat{C}_{ij} T_j + \sum_{j=N+1}^{N+n} \hat{R}_{ij} T_j^4, \qquad i = 1, \ldots, N \quad (5)$$

After making these substitutions, the thermal network equation (1) is written in the more compact form

$$F(T) \equiv Q + CT + RD(T) = 0 \quad (6)$$

Assume that temperature measurements can be taken at M nodes of the network. These are the observed nodes of the system, denoted as the α set. The remaining $N - M$ nodes are the unobservable nodes of the system, denoted as the β set. Let $\boldsymbol{T}_\alpha$ denote the set of measured temperatures at the observed nodes. Finally, assume that the nodes of the system have been rearranged so that the temperature vector $\boldsymbol{T}$ can be partitioned as $\boldsymbol{T} = [\boldsymbol{T}_\alpha, \boldsymbol{T}_\beta]$, where $\boldsymbol{T}_\alpha$ is the temperature vector of the α set and $\boldsymbol{T}_\beta$ is the temperature vector of the β set. Then system (6) can be partitioned as

$$\begin{bmatrix} \boldsymbol{F}_1(\boldsymbol{T}_\alpha, \boldsymbol{T}_\beta) \\ \boldsymbol{F}_2(\boldsymbol{T}_\alpha, \boldsymbol{T}_\beta) \end{bmatrix} = \begin{bmatrix} \boldsymbol{Q}_\alpha \\ \boldsymbol{Q}_\beta \end{bmatrix} + \begin{bmatrix} C_{\alpha\alpha} & C_{\alpha\beta} \\ C_{\beta\alpha} & C_{\beta\beta} \end{bmatrix} \begin{bmatrix} \boldsymbol{T}_\alpha \\ \boldsymbol{T}_\beta \end{bmatrix} + \begin{bmatrix} R_{\alpha\alpha} & R_{\alpha\beta} \\ R_{\beta\alpha} & R_{\beta\beta} \end{bmatrix} \begin{bmatrix} D(\boldsymbol{T}_\alpha) \\ D(\boldsymbol{T}_\beta) \end{bmatrix} = \begin{bmatrix} 0 \\ 0 \end{bmatrix} \quad (7)$$

where $C_{\alpha\alpha}$ and $R_{\alpha\alpha}$ are the $M \times M$ principal submatrices of C and R and $C_{\beta\beta}$ and $R_{\beta\beta}$ are $(N - M) \times (N - M)$ submatrices of C and R, respectively.

Heuristically the problem that is addressed is to estimate the temperature set $\boldsymbol{T}_\beta$ from the model (7) and (noisy) temperature measurements at the observed nodes. Various estimators of $\boldsymbol{T}_\beta$ can be obtained based on a priori knowledge assumptions made on the loads $\boldsymbol{Q}$ in the model and the error in the measured temperature values. To explore these possibilities a few model problems are first described that will serve to guide the development of these formulations.

A. Model Problems

The estimation problems discussed are restricted to linear models. This serves not only to simplify the exposition, but also to identify the linearized subproblems that are associated with solving the nonlinear estimation problem via iterative methods.

The simplest (and probably earliest) expansion technique is due to Guyan.[3] Although its original application is to structural models, because it only involves the stiffness matrix of the system, it has an analogous application to steady-state linear conduction models. The correspondences are 1) conduction matrix → stiffness matrix, 2) temperature → displacement, and 3) heat flow rate → force. The Guyan expansion is based on the assumption that the state of the system is due to loads applied at the observed nodes. Thus, in the Guyan model, system (7) has the form

$$\begin{bmatrix} C_{\alpha\alpha} & C_{\alpha\beta} \\ C_{\beta\alpha} & C_{\beta\beta} \end{bmatrix} \begin{bmatrix} \boldsymbol{T}_\alpha \\ \boldsymbol{T}_\beta \end{bmatrix} + \begin{bmatrix} \boldsymbol{Q}_\alpha \\ 0 \end{bmatrix} = 0 \quad (8)$$

where, by our correspondences, $\boldsymbol{T}$ is the deformation and $\boldsymbol{Q}_\alpha$ is the force. $\boldsymbol{T}_\alpha$ is known with certainty in this model, and $\boldsymbol{Q}_\beta$ is known to be zero. The solution for the displacements at the β set is now deterministic:

$$\boldsymbol{T}_\beta = -C_{\beta\beta}^{-1} C_{\beta\alpha} \boldsymbol{T}_\alpha \quad (9)$$

Note that it is not necessary to know the value of $\boldsymbol{Q}_\alpha$ to determine $\boldsymbol{T}_\beta$, only that $\boldsymbol{Q}_\beta = 0$. In fact, $\boldsymbol{Q}_\alpha$ can be solved for after $\boldsymbol{T}_\beta$ is determined.

The Guyan[3] assumptions are fairly restrictive in that error in the measured temperatures are not allowed, and zero load at the β set is assumed. These assumptions can be relaxed once it is recognized that the Guyan expansion solves a certain optimization problem. The optimization perspective opens up several alternatives for dealing with departures from the nominal assumptions. These are described next.

Let P_α denote the projection operator onto the α set, that is,

$$P_\alpha \begin{bmatrix} \boldsymbol{T}_\alpha \\ \boldsymbol{T}_\beta \end{bmatrix} = \boldsymbol{T}_a \quad (10)$$

for any displacement vector $\boldsymbol{T} = [\boldsymbol{T}_\alpha, T_\beta]$. By direct substitution, it is easy to verify that

$$\boldsymbol{T} = \begin{bmatrix} \hat{\boldsymbol{T}} \\ -C_{\beta\beta}^{-1} C_{\beta\alpha} \hat{\boldsymbol{T}} \end{bmatrix} \quad (11)$$

solves the optimization problem

$$\min_T \langle C\boldsymbol{T}, \boldsymbol{T} \rangle, \qquad \text{subject to} \qquad \hat{\boldsymbol{T}} = P_\alpha \boldsymbol{T} \quad (12)$$

where $\hat{\boldsymbol{T}}$ represents the measured temperatures. This result states that the Guyan[3] expansion is obtained by minimizing the strain energy of the system while constraining the α set displacements to match

the measured displacement vector $\hat{\boldsymbol{T}}$. Although the initial Guyan assumption on the applied force may have appeared to be ad hoc, it is now a consequence of the solution to the optimization problem.

The optimization formulation makes it quite natural to incorporate errors in the measurement $\hat{\boldsymbol{T}}$. For example, a standard quadratic programming problem results if the constraint $\boldsymbol{y} = P_\alpha \boldsymbol{T}$ is replaced by the M inequality constraints, where M is the number of observed nodes:

$$|\hat{T}_i - T_i| \leq \epsilon_i, \qquad i = 1, \ldots, M \tag{13}$$

where $\epsilon_i \geq 0$ defines the maximum allowable error in each measurement. A scalar constraint of the form

$$|\hat{\boldsymbol{T}} - \boldsymbol{T}_\alpha|^2 \leq \epsilon \tag{14}$$

leads to the LSQI problem,[15] which will be analyzed in greater detail in Sec. IV.

The solution can also be affected by changing the objective functional. For example, inserting the cost functional $J(\boldsymbol{T}) \equiv |C\boldsymbol{T}|^2$ into relation (12) leads to a solution to the equality constrained problem (12) that no longer constrains the applied forces to the observed nodes. The solution to this problem minimizes the Euclidean norm of the vector of forces required to obtain the measured displacements. Still another option is to introduce the constraint via a penalty function, for example,

$$\min_T \langle C\boldsymbol{T}, \boldsymbol{T}\rangle + \gamma |P_\alpha \boldsymbol{T} - \hat{\boldsymbol{T}}|^2 \tag{15}$$

for suitably chosen scalar weighting term γ.

The preceding various optimization alternatives make no a priori assumptions on the applied load. The thermal network problems always involve a heat load entering through the boundary conditions in addition to other possible sources. If the load is known with certainty, the problem is totally determined; we simply solve the system

$$C\boldsymbol{T} + \boldsymbol{Q} = 0 \tag{16}$$

where $\boldsymbol{Q}$ is the applied load. Equation (16) has equivalent formulations as optimization problems, for example, when C is positive definite, an equivalent formulation is

$$\min_T \langle C\boldsymbol{T}, \boldsymbol{T}\rangle + 2\langle \boldsymbol{T}, \boldsymbol{Q}\rangle \tag{17}$$

Another formulation is

$$\min_T |C\boldsymbol{T} + \boldsymbol{Q}|^2 \tag{18}$$

In the mechanical system, the first formulation in relation (17) minimizes the energy imbalance under the assumed load, whereas the objective (18) minimizes the force imbalance under the load. These quadratic forms can be substituted into the various optimization problems that have been formulated to account for a priori knowledge of the load. Coupled with the constraint equations in Eq. (12), (13), or (14), the minimum value of these objective functionals will not necessarily be zero.

A final alternative that is worthwhile to discuss uses a probabilistic formulation of the problem. In this case, we write the load as $\boldsymbol{Q} = \boldsymbol{Q}_0 + \delta\boldsymbol{Q}$, where $\boldsymbol{Q}_0$ is known and $\delta\boldsymbol{Q}$ is an unknown random vector with known covariance matrix $d\boldsymbol{Q}$. The corresponding displacement can be written as $\boldsymbol{T} = \boldsymbol{T}_0 + \delta\boldsymbol{T}$, where $\boldsymbol{T}_0 = -C^{-1}\boldsymbol{Q}_0$ and $\delta\boldsymbol{T} = -C^{-1}\delta\boldsymbol{Q}$. The measurement equation has the form

$$\hat{\boldsymbol{T}} = P_\alpha \boldsymbol{T} + \boldsymbol{\eta} \tag{19}$$

where $\boldsymbol{\eta}$ is a measurement error vector with known covariance matrix, for example, R_η. When $z = \hat{T} - P_\alpha T_0$, the estimation problem is to find the linear minimum variance estimate of $\delta\boldsymbol{T}$ given the measurement $z = P_\alpha \delta\boldsymbol{T} + \boldsymbol{\eta}$ and the covariance matrix

$$E(\delta\boldsymbol{T}\delta\boldsymbol{T}^T) = C^{-1} d\boldsymbol{Q} C^{-T} \tag{20}$$

This is a standard Gauss–Markov estimation problem and is equivalent to the weighted least-squares problem

$$\min_{\delta T} \left[\delta\boldsymbol{T}^T C^T d\boldsymbol{Q}^{-1} C\delta\boldsymbol{T} + (z - P_\alpha \delta\boldsymbol{T})^T R_\eta^{-1} (z - P_\alpha \delta\boldsymbol{T})^T\right] \tag{21}$$

Note that this formulation is very similar to the weighted problem (17).

B. Network Estimation Problems

The extension of any of these formulations to the nonlinear model in Eq. (7) will require iterative solutions that involve solving linear subproblems of the type described earlier. An important consideration in the choice of problem formulation is the difficulty in solving the linearized subproblems. Because of the nature of the thermal network, the objective functional must contain some a priori information of applied heat loads because they will at least be present via the boundary conditions.

The weighted least-squares problem (17) satisfies both requirements. Furthermore, it enjoys an "optimal" probabilisitic interpretation when the weighting parameters properly reflect the covariance matrices of the process noise term $d\boldsymbol{Q}$ and the measurement noise term R_η. Although it is reasonable to assume that the statistics of the measurement error may be fairly well characterized, the same probably cannot be assumed about the load. In the absence of statistics on the load vector, the weights tend to become somewhat arbitrary. In this case the inequality constrained formulations are preferable. These formulations enforce the assumed measurement error without weighing the magnitude of this error against the accuracy of the thermal model with its assumed load.

These considerations lead us to define two problems, both based on minimizing an error imbalance subject to the scalar inequality constraint (14). The choice of the LSQI constraint instead of the constraint in relation (13) is for simplicity in solving the linearized subproblems without sacrificing the constrained measurement error formulation. The first objective formulation is an extension of the Guyan[3] model. The interpretation is that there are two observed parts of the model. The first is the α set of temperatures, and the second is the load applied to the β set. Hence, this formulation assumes that the correct load has been applied to the β set, $\boldsymbol{Q}_\beta$. This problem will henceforth be referred to as nonlinear programming problem 1 (NP1).

Problem NP1:

$$\min_T |\boldsymbol{F}_1(\boldsymbol{T})|^2 \tag{22}$$

[compare Eq. (7)], subject to

$$\boldsymbol{F}_2(\boldsymbol{T}) = 0 \tag{23}$$

$$|\boldsymbol{T}_\alpha - \hat{\boldsymbol{T}}|^2 \leq \epsilon |\hat{\boldsymbol{T}}|^2 \tag{24}$$

Note that, if $\epsilon = 0$ (absence of noise in the measurements), this problem reduces to the Guyan expansion[3] that was described earlier.

The second formulation does not make this assumption and is referred to as NP2.

Problem NP2:

$$\min_T \boldsymbol{F}(\boldsymbol{T}) = |C\boldsymbol{T} + RD(\boldsymbol{T}) + \boldsymbol{Q}|^2 \tag{25}$$

subject to

$$|\boldsymbol{T}_\alpha - \hat{\boldsymbol{T}}|^2 \leq \epsilon |\hat{\boldsymbol{T}}|^2 \tag{26}$$

Problem NP2 is more consistent with the assumption that the entire load vector $\boldsymbol{Q}$ might need modification; hence, to rectify the discrepancy between measured and computed temperatures at the observed nodes, heat may be applied anywhere. The robustness and overall efficiency of these two strategies are discussed in Sec. V, where numerical tests of the various algorithms are described.

III. Standard Algorithms for Estimation Problems NP1 and NP2

In this section, a standard approach for solving problems NP1 and NP2 will be discussed. In the next section improved algorithms that take advantage of the particular structure of the equations will be presented. Problems NP1 and NP2 are examples of the general NP problem. The problem is formulated as follows.

Consider a continuously differentiable objective function $f(\boldsymbol{x}): \mathbb{R}^n \to \mathbb{R}$, and m continuously differentiable functions $c_j(\boldsymbol{x}): \mathbb{R}^n \to \mathbb{R}$, $j = 1, \ldots, m$, that serve as equality and/or inequality constraints. The constraints are assumed to satisfy some qualifications, also referred to as regularity conditions (for example, see Fletcher[17] and Gill et al.[18]). These qualifications are typically satisfied in practical applications. The general NP problem is defined as follows.

Problem NP:

$$\min_{x} f(\boldsymbol{x}) \tag{27}$$

subject to

$$c_j(\boldsymbol{x}) \leq 0, \qquad j = 1, \ldots, m \tag{28}$$

The associated Lagrangian is defined as

$$L(\boldsymbol{x}, \lambda) = f(\boldsymbol{x}) - \sum_{j=1}^{m} \lambda_j c_j(\boldsymbol{x}) \tag{29}$$

The solutions to the preceding problem satisfy the well-known Kuhn–Tucker optimality conditions

$$\frac{\partial L(\boldsymbol{x}, \lambda)}{\partial \boldsymbol{x}_i} = 0, \qquad i = 1, \ldots, N \tag{30}$$

$$\lambda_j \cdot c_j(\boldsymbol{x}) = 0, \qquad j = 1, \ldots, m \tag{31}$$

$$\lambda_j \leq 0, \qquad c_j(\boldsymbol{x}) \leq 0, \qquad j = 1, \ldots, m \tag{32}$$

where λ_j, $j = 1, \ldots, m$, are the Lagrange multipliers of the problem.

Over the years, numerous methods have been developed for the numerical solution of problem NP. Most of these methods are based on some iterative procedure to identify points where the Kuhn–Tucker conditions hold. Among them, the SQP method[19,20] is probably the most popular due to its robustness and good convergence properties. According to this method, the sequence of approximations is generated by solving at each step the quadratic programming subproblem that results from quadratic approximation of the Lagrangian and linearization of the constraints. Modifications and upgrades to the original SQP were proposed by Fletcher,[21] Burke and Han,[22] Sahba,[23] and others.

In the course of the present study, the algorithms that solve problems NP1 and NP2 have been implemented in a MATLAB® code, which employs the built-in SQP routine of MATLAB.[24] The SQP method requires the computation of the solution to the thermal network equations (6) and its Jacobian during each step of the iteration procedure. The network equations are solved with the algorithm of Milman and Petrick,[13] which is based on a restricted step-size Newton method. The Newton iterates are evaluated along a descent direction of $|F(\boldsymbol{T})|^2$. The step size of each iteration is determined via a backtracking line-search algorithm.[25] An important cost-saving feature of the thermal solver is the analytic evaluation of the Jacobian of the thermal network equations (or semi-analytic, in the case of temperature-dependent conductance matrices C and R).

Nonetheless, the SQP-based algorithms for NP1 and NP2 might still be very slow for large-scale optimization problems, such as those that are most often encountered in practical applications. (Typically a thermal network consists of thousands of nodes.) The reasons for the slow performance of these algorithms are as follows: 1) they use approximate expressions for the Lagrangian and its derivatives, 2) they use approximate (linearized) expressions for the constraints, and 3) they require the solution of the thermal network equations during each step of the iteration procedure. It is, therefore, desired to develop some alternative methods with improved speed for the solutions of the problems of interest. The proposed algorithms and their numerical implementations are described in detail in the following section.

IV. Fast Algorithms for Estimation Problems NP1 and NP2

The basic idea of the proposed methods for the solution of the optimization problems of interest is to construct a Gauss–Newton iteration procedure that takes advantage of the form of constraints (24) and (26) and converges quadratically to the desired solution.

Assume an objective function $|f(\boldsymbol{x})|^2$ and m constraints $c_j(\boldsymbol{x})$, $j = 1, \ldots, m$. Given a current iterate $\boldsymbol{x}^k$, the Gauss–Newton procedure computes the next approximation to the solution, $\boldsymbol{x}^{k+1}$, as the solution of the following quadratic programming (QP) problem (for example, see Ref. 18):

$$\min_{x^{k+1}} |f(\boldsymbol{x}^k) + (\boldsymbol{x}^{k+1} - \boldsymbol{x}^k)^T \cdot \nabla f(\boldsymbol{x}^k)|^2 \tag{33}$$

subject to

$$c_j(\boldsymbol{x}^{k+1}) \leq 0, \qquad j = 1, \ldots, m \tag{34}$$

The starting point of the sequence can be the solution of $f(\boldsymbol{x}) = 0$ in the absence of constraints, that is, $\{x^0 \in \mathbb{R}^N : f(x^0) = 0\}$. This algorithm converges if the starting point is sufficiently close to a solution of the problem. The convergence rate is quadratic, provided that the Jacobian $\nabla f(\boldsymbol{x}^k)$ is invertible.

A. Gauss–Newton Algorithm for Problem NP1

First assume that at least one node of the β set exchanges heat with either the boundary or at least one node from the α set. This assumption implies that the β set is not isolated from both the α set and the boundary, and it holds for all nontrivial thermal systems. It has been shown[14] that under the preceding assumption the equation $\boldsymbol{F}_2(\boldsymbol{T}_\alpha, \boldsymbol{T}_\beta) = 0$ possesses a unique solution $\boldsymbol{T}_\beta > 0$ for every $\boldsymbol{T}_\alpha > 0$. In other words, the first equation of Eq. (7) defines a continuous function $\mathbb{R}_+^M \to \mathbb{R}_+^M : \boldsymbol{T}_\beta = \boldsymbol{T}_\beta(\boldsymbol{T}_\alpha)$. This function can be employed to eliminate the temperatures of the unobservable nodes from the expression of $\boldsymbol{F}_1$ in Eq. (7):

$$\boldsymbol{F}_1 = \boldsymbol{F}_1[\boldsymbol{T}_\alpha, \boldsymbol{T}_\beta(\boldsymbol{T}_\alpha)] \tag{35}$$

with

$$\nabla \boldsymbol{F}_1 = \left(\frac{\partial \boldsymbol{F}_1}{\partial \boldsymbol{T}_\alpha}\right) - \left(\frac{\partial \boldsymbol{F}_1}{\partial \boldsymbol{T}_\beta}\right)\left(\frac{\partial \boldsymbol{F}_2}{\partial \boldsymbol{T}_\beta}\right)^{-1}\left(\frac{\partial \boldsymbol{F}_2}{\partial \boldsymbol{T}_\alpha}\right) \tag{36}$$

In view of these relations, the Gauss–Newton algorithm that generates the iterates $\{T^k\}$ consists of the following steps:

1) Given a thermal network model and boundary conditions, solve the system of equations (7) to evaluate the starting point $[\boldsymbol{T}_\alpha^0, \boldsymbol{T}_\beta^0]$.

2) Given an iterate $[\boldsymbol{T}_\alpha^k, \boldsymbol{T}_\beta^k]$, compute $\boldsymbol{T}_\alpha^{k+1}$ by solving the following linear least-squares problem with quadratic constraint (LSQ1):

Problem LSQ1

$$\min_{T_\alpha} \left|\boldsymbol{F}_1\left(\boldsymbol{T}_\alpha^k, \boldsymbol{T}_\beta^k\right) + \left(\boldsymbol{T}_\alpha - \boldsymbol{T}_\alpha^k\right)^T \cdot (\nabla \boldsymbol{F}_1)^k\right|^2 \tag{37}$$

subject to

$$|T_\alpha - \hat{T}|^2 \leq \epsilon |\hat{T}|^2 \tag{38}$$

3) When $\boldsymbol{T}_\alpha^{k+1}$ is computed, evaluate $\boldsymbol{T}_\beta^{k+1}$ as the solution of the nonlinear system

$$\boldsymbol{F}_2\left(\boldsymbol{T}_\alpha^{k+1}, \boldsymbol{T}_\beta\right) = 0 \tag{39}$$

where $\boldsymbol{F}_2$ is given by Eq. (7). An alternative approach for the computation of $\boldsymbol{T}_\beta^{k+1}$ is to solve the linearized version of the preceding system,

$$\boldsymbol{F}_2\left(\boldsymbol{T}_\alpha^k, \boldsymbol{T}_\beta^k\right) + \left(\boldsymbol{T}_\alpha^{k+1} - \boldsymbol{T}_\alpha^k\right)^T \cdot \left(\frac{\partial \boldsymbol{F}_2}{\partial \boldsymbol{T}_\alpha}\right)^k + \left(\boldsymbol{T}_\beta - \boldsymbol{T}_\beta^k\right)^T \cdot \left(\frac{\partial \boldsymbol{F}_2}{\partial \boldsymbol{T}_\beta}\right)^k = 0 \tag{40}$$

This alternative approach for $\boldsymbol{T}_\beta^{k+1}$ produces considerable savings in computing time because it avoids the iterative procedure that is required for the numerical solution of the nonlinear system (39).

Step 2 is an optimization problem in itself and is the key step in the proposed procedure. Its solution will be discussed now in detail. When the substitutions

$$\tilde{\boldsymbol{T}}_\alpha = \boldsymbol{T}_\alpha - \hat{\boldsymbol{T}}, \qquad \tilde{\epsilon} = \epsilon|\hat{\boldsymbol{T}}|^2 \tag{41}$$

$$\tilde{C} \equiv \begin{bmatrix} \tilde{C}_{\alpha\alpha} & \tilde{C}_{\alpha\beta} \\ \tilde{C}_{\beta\alpha} & \tilde{C}_{\beta\beta} \end{bmatrix} = \begin{bmatrix} C_{\alpha\alpha} & C_{\alpha\beta} \\ C_{\beta\alpha} & C_{\beta\beta} \end{bmatrix} + 4 \begin{bmatrix} R_{\alpha\alpha} & R_{\alpha\beta} \\ R_{\beta\alpha} & R_{\beta\beta} \end{bmatrix} \begin{bmatrix} D'\left(\boldsymbol{T}_\alpha^k\right) \\ D'\left(\boldsymbol{T}_\beta^k\right) \end{bmatrix} \tag{42}$$

$$\tilde{\boldsymbol{Q}} \equiv \begin{bmatrix} \tilde{\boldsymbol{Q}}_\alpha \\ \tilde{\boldsymbol{Q}}_\beta \end{bmatrix} = \begin{bmatrix} \boldsymbol{Q}_\alpha \\ \boldsymbol{Q}_\beta \end{bmatrix} - 3 \begin{bmatrix} R_{\alpha\alpha} & R_{\alpha\beta} \\ R_{\beta\alpha} & R_{\beta\beta} \end{bmatrix} \begin{bmatrix} D\left(\boldsymbol{T}_\alpha^k\right) \\ D\left(\boldsymbol{T}_\beta^k\right) \end{bmatrix} \tag{43}$$

$$\tilde{A} = \tilde{C}_{\alpha\alpha} - \tilde{C}_{\alpha\beta}\tilde{C}_{\beta\beta}^{-1}\tilde{C}_{\beta\alpha} \tag{44}$$

$$\tilde{B} = \tilde{A}\hat{\boldsymbol{T}} + \tilde{\boldsymbol{Q}}_\alpha - \tilde{C}_{\alpha\beta}\tilde{C}_{\beta\beta}^{-1}\tilde{\boldsymbol{Q}}_\beta \tag{45}$$

are made, the linearized problem LSQ1 can be written as

$$\min_{\tilde{T}_\alpha} |\tilde{A}\tilde{\boldsymbol{T}}_\alpha + \tilde{B}|^2 \tag{46}$$

subject to

$$|\tilde{\boldsymbol{T}}_\alpha|^2 \le \tilde{\epsilon} \tag{47}$$

Note that the Jacobian $\nabla \boldsymbol{F}_1$ [Eq. (37)] is nonvanishing for every $\boldsymbol{T}_\alpha > 0$ (Ref. 14). Therefore, $\tilde{A}$ is always invertible.

The preceding optimization problem can be solved via standard algorithms that involve the singular value decomposition (SVD) of $\tilde{A}$ (for example, see Golub and Van Loan[15]). However, the SVD is computationally expensive. (Essentially, it is an eigenvalue-finding procedure.) Therefore, large-scale iteration schemes that employ the SVD can often be very slow. The algorithm to be described replaces the SVD with the QR decomposition, which is a much faster procedure. Flop count comparisons between the two decompositions[15] indicate that the QR decomposition can be up to 20 times faster than the SVD.

Let L_1 denote the Lagrangian of problem LSQ1 (46) and (47). Then,

$$L_1 = |\tilde{A}\tilde{\boldsymbol{T}}_\alpha + \tilde{B}|^2 + \lambda\left(|\tilde{\boldsymbol{T}}_\alpha|^2 - \tilde{\epsilon}\right) \tag{48}$$

where λ is the Lagrange multiplier of the problem. The Kuhn–Tucker optimality conditions for this problem are

$$(\tilde{A}^T\tilde{A} + \lambda I)\tilde{\boldsymbol{T}}_\alpha = -\tilde{A}^T\tilde{B} \tag{49}$$

$$\lambda\left(|\tilde{\boldsymbol{T}}_\alpha|^2 - \tilde{\epsilon}\right) = 0 \tag{50}$$

$$|\tilde{\boldsymbol{T}}_\alpha|^2 - \tilde{\epsilon} \le 0 \tag{51}$$

$$\lambda \le 0 \tag{52}$$

First, assume that the solution lies inside the feasibility region, that is, $|\tilde{\boldsymbol{T}}_\alpha|^2 < \tilde{\epsilon}$. Then condition (50) implies that $\lambda = 0$. In this case, it is immediately deduced from Eq. (49) that

$$\tilde{\boldsymbol{T}}_\alpha^{k+1} = -\tilde{A}^{-1}\tilde{B} \tag{53}$$

Next, assume that the solution lies on the boundary of the feasibility region, that is, $|\tilde{\boldsymbol{T}}_\alpha|^2 = \tilde{\epsilon}$. Let Θ be an orthogonal matrix and Z be an upper triangular matrix such that $\tilde{A} = \Theta Z$. Because Z^TZ is symmetric, there is an orthonormal matrix Φ such that $\Phi^T Z^T Z \Phi = \Lambda$, where Λ is diagonal. Therefore, Eq. (44) can be written as

$$\Phi(\Lambda + \lambda I)\Phi^T\tilde{\boldsymbol{T}}_\alpha = -\tilde{A}^T\tilde{B} \tag{54}$$

This equation can be solved for $\tilde{\boldsymbol{T}}_\alpha$ and inserted into Eq. (45). The result is

$$d_1(\lambda) = |\Phi(\Lambda + \lambda I)^{-1}\Phi^T\tilde{A}^T\tilde{B}|^2 = \tilde{\epsilon} \tag{55}$$

This is a secular equation and can be solved in $\mathcal{O}(M)$ operations. It is evident that $d_1(\lambda)$ is a continuous function and monotonic.[15] Therefore, for a given $\tilde{\epsilon}$, there exists a unique solution, for example, λ^*. Because $d_1(\lambda)$ is monotonic, a simple bisection approach can be used to compute λ^*. After the value of λ^* has been obtained, the optimal vector $\tilde{\boldsymbol{T}}_\alpha$ is obtained from Eq. (49).

Once the iterate for the observed nodes $\boldsymbol{T}_\alpha^{k+1}$ has been computed as the solution of the LSQ1 problem, the iterate of the unobservable nodes $\boldsymbol{T}_\beta^{k+1}$ can be directly evaluated by solving the linear system of step 3 [Eq. (40)]. When relationships (42) and (45) are employed, the expression for the iterate becomes

$$\boldsymbol{T}_\beta^{k+1} = -\tilde{C}_{\beta\beta}^{-1}\left(\tilde{\boldsymbol{Q}}_\beta + \tilde{C}_{\beta\alpha}\boldsymbol{T}_\alpha^{k+1}\right) \tag{56}$$

Note that the described Gauss–Newton algorithm converges only locally. If global convergence is desired, the algorithm must be supplemented by an appropriate line-search procedure that limits the step size. The starting point $\boldsymbol{T}_0$, however, is the solution to the initial thermal network equations (6), and so it is expected to be sufficiently close to the optimal solution even when the available thermal model is moderately accurate. Therefore, the use of line-search procedures can be avoided in almost all practical applications, resulting in significant savings in computing time.

B. Gauss–Newton Algorithm for Problem NP2

Consider the full system of Eqs. (6) and the problem NP2 [Eqs. (25) and (26)]. The Gauss–Newton algorithm that generates the iterates $\{T^K\}$ consists of the following steps:

1) Given a thermal network model and boundary conditions, solve the system of equations (6) to evaluate the starting point $\boldsymbol{T}^0 = [\boldsymbol{T}_\alpha^0 \;\; \boldsymbol{T}_\beta^0]$.

2) Given an iterate $\boldsymbol{T}^k = [\boldsymbol{T}_\alpha^k \;\; \boldsymbol{T}_\beta^k]$, compute the next iterate $\boldsymbol{T}^{k+1} = [\boldsymbol{T}_\alpha^{k+1} \;\; \boldsymbol{T}_\beta^{k+1}]$ by solving the following linear least-squares problem with quadratic constraint LSQ2:

Problem LSQ2

$$\min_T |F(\boldsymbol{T}) + (\boldsymbol{T} - \boldsymbol{T}^k)^T \cdot (\nabla F)^k|^2 \tag{57}$$

subject to

$$|P\boldsymbol{T} - \hat{\boldsymbol{T}}|^2 \le \epsilon|\hat{\boldsymbol{T}}|^2 \tag{58}$$

where P is the $M \times N$ matrix that selects the observed nodes, that is, $P\boldsymbol{T} = \boldsymbol{T}_\alpha$. Without loss of generality, it may be assumed that P has the form

$$P = [I_\alpha \quad 0] \tag{59}$$

where I_α is the $M \times M$ identity matrix. When the following substitutions are made:

$$\tilde{\boldsymbol{T}} = \boldsymbol{T} - [\hat{\boldsymbol{T}} \quad 0]^T \qquad \tilde{\epsilon} = \epsilon|\hat{\boldsymbol{T}}|^2 \tag{60}$$

and relations (42) and (43) are employed, problem LSQ2 can be rewritten as

$$\min_{\tilde{T}} |\tilde{C}\tilde{\boldsymbol{T}} + \tilde{\boldsymbol{Q}}'|^2 \tag{61}$$

subject to

$$|P\tilde{\boldsymbol{T}}|^2 \le \tilde{\epsilon} \tag{62}$$

where

$$\tilde{\boldsymbol{Q}}' = \tilde{\boldsymbol{Q}} + \tilde{C} \cdot [\hat{\boldsymbol{T}} \quad 0]^T \tag{63}$$

Note that the matrix $\tilde{C} = \tilde{C}(\boldsymbol{T}_\alpha^k, \boldsymbol{T}_\beta^k)$, defined in Eq. (42), is the Jacobian of the function $F(\boldsymbol{T})$, Eq. (6). It has been shown by Milman and Petrick[13] that this matrix is invertible for every $\boldsymbol{T} > 0$.

The LSQ2 problem can also be solved by the standard algorithm[15] that is based on the generalized SVD decomposition of the augmented matrix $[\tilde{C}, P]$. However, as mentioned earlier, this operation can be very costly. It is, therefore, desirable to design a faster numerical procedure by exploiting the particular structure of the matrices involved. Such a procedure is described next.

The Lagrangian of this problem is

$$L_2 = |\tilde{C}\tilde{\boldsymbol{T}} + \tilde{\boldsymbol{Q}}'|^2 + \lambda(|\tilde{\boldsymbol{T}}|^2 - \tilde{\epsilon}) \tag{64}$$

and the Kuhn–Tucker optimality conditions are

$$\left(\tilde{C}^T\tilde{C} + \lambda\tilde{I}_\alpha\right)\tilde{\boldsymbol{T}} = -\tilde{C}^T\tilde{\boldsymbol{Q}}' \tag{65}$$

$$\lambda(|\tilde{\boldsymbol{T}}|^2 - \tilde{\epsilon}) = 0 \tag{66}$$

$$|\tilde{\boldsymbol{T}}|^2 - \tilde{\epsilon} \le 0 \tag{67}$$

$$\lambda \le 0 \tag{68}$$

where

$$\tilde{I}_\alpha = P^T P = \begin{bmatrix} I_\alpha & 0 \\ 0 & 0 \end{bmatrix} \tag{69}$$

As in the case of LSQ1, if a Kuhn–Tucker point lies inside the feasibility region, then condition (66) implies that $\lambda = 0$. Then it is deduced from condition (65) that

$$\tilde{\boldsymbol{T}}^{k+1} = -\tilde{C}^{-1}\tilde{\boldsymbol{Q}}' \tag{70}$$

If the optimal solution lies on the boundary of the feasibility region, the proposed numerical procedure is the following. Consider the QR factorization $\tilde{C} = \Omega\Gamma$, where Ω is orthogonal and Γ is lower triangular. Γ is partitioned as

$$\Gamma = \begin{bmatrix} \Gamma_{\alpha\alpha} & 0 \\ \Gamma_{\beta\alpha} & \Gamma_{\beta\beta} \end{bmatrix} \tag{71}$$

Obviously, $\tilde{C}^T\tilde{C} = \Gamma^T\Gamma$, so that $\Gamma^T\Gamma$ is the Cholesky factorization of $\tilde{C}^T\tilde{C}$. Then, optimality condition (66) becomes

$$\Gamma^T\left(I + \lambda\Gamma^{-T}\tilde{I}_\alpha\Gamma^{-1}\right)\Gamma\tilde{\boldsymbol{T}} = -\tilde{C}^T\tilde{\boldsymbol{Q}}' \tag{72}$$

When $\psi = \Gamma\tilde{\boldsymbol{T}}$ is defined, Eq.(72) becomes

$$\left(I + \lambda\Gamma^{-T}\tilde{I}_\alpha\Gamma^{-1}\right)\psi = -\Omega^T\tilde{\boldsymbol{Q}}' \tag{73}$$

Because Γ is lower triangular, its inverse, denoted by $\tilde{\Gamma}$, has the form

$$\Gamma^{-1} \equiv \tilde{\Gamma} = \begin{bmatrix} \tilde{\Gamma}_{\alpha\alpha} & 0 \\ \tilde{\Gamma}_{\beta\alpha} & \tilde{\Gamma}_{\beta\beta} \end{bmatrix} \tag{74}$$

so that

$$\Gamma^{-T}\tilde{I}_\alpha\Gamma^{-1} = \begin{bmatrix} \tilde{\Gamma}_{\alpha\alpha}^T\tilde{\Gamma}_{\alpha\alpha} & 0 \\ 0 & 0 \end{bmatrix} \tag{75}$$

When ψ is partitioned as $\psi = [\psi_\alpha, \psi_\beta]^T$ and $\Omega^T\tilde{\boldsymbol{Q}}'$ is partioned as $\Omega^T\tilde{\boldsymbol{Q}}' = [\boldsymbol{\omega}_\alpha \;\; \boldsymbol{\omega}_\beta]^T$, system (73) can be written as

$$\left(I_\alpha + \lambda\tilde{\Gamma}_{\alpha\alpha}^T\tilde{\Gamma}_{\alpha\alpha}\right)\psi_\alpha = -\boldsymbol{\omega}_\alpha \tag{76}$$

$$\psi_\beta = -\boldsymbol{\omega}_\beta \tag{77}$$

Because $\tilde{\Gamma}_{\alpha\alpha}^T\tilde{\Gamma}_{\alpha\alpha}$ is symmetric, there is an orthonormal matrix U such that

$$U^T\Gamma_{\alpha\alpha}^T\Gamma_{\alpha\alpha}U = \tilde{D} \tag{78}$$

where $\tilde{D}$ is diagonal. Furthermore, the diagonal elements of $\tilde{D}$ are strictly positive because Γ is invertible. Now, because $\tilde{\Gamma}_{\alpha\alpha} = \Gamma_{\alpha\alpha}^{-1}$ (recall that Γ is lower triangular), inverting Eq. (78) yields $U^T\tilde{\Gamma}_{\alpha\alpha}^T\tilde{\Gamma}_{\alpha\alpha}U = \tilde{D}^{-1}$. Thus, diagonalization of Eq. (76) results in

$$\psi_\alpha = -U\left(I_\alpha + \lambda\tilde{D}^{-1}\right)U^T\boldsymbol{\omega}_\alpha \tag{79}$$

Partitioning $\tilde{\boldsymbol{T}}$ as $\tilde{\boldsymbol{T}} = [\tilde{\boldsymbol{T}}_\alpha, \tilde{\boldsymbol{T}}_\beta]$, one gets [compare Eq. (74)]

$$\psi_\alpha = \Gamma_{\alpha\alpha}\tilde{\boldsymbol{T}}_\alpha \tag{80}$$

Substituting Eqs. (79) and (80) to the optimality condition (66), one finally arrives at the following secular equation, analogous to Eq. (55):

$$d_2(\lambda) \equiv \left|\tilde{\Gamma}_{\alpha\alpha}U\left(I_\alpha + \lambda\tilde{D}^{-1}\right)U^T\boldsymbol{\omega}_\alpha\right|^2 = \tilde{\epsilon} \tag{81}$$

The function $d_2(\lambda)$ is also monotonic, and therefore, a simple bisection approach can be used to solve Eq. (81) for λ. Once the value of λ has been obtained, for example, λ^*, then ψ_α can be computed from Eq. (79). On the other hand, ψ_β is directly evaluated from Eq. (77). Therefore, the next iterate of $\boldsymbol{T}$, $\boldsymbol{T}^{k+1}$ is given by

$$\boldsymbol{T}^{k+1} = \tilde{\Gamma}\psi + [\hat{\boldsymbol{T}} \quad 0]^T \tag{82}$$

The factorization of $\tilde{C}$ is an $\mathcal{O}(N^3)$ problem (although this can be accelerated by using fast Givens rotations to take advantage of sparsity and bandedness), and the diagonalization problem is $\mathcal{O}(M^3)$. In numerical tests performed in the context of the present study, it was observed that a speedup of a factor of 30 or greater can be achieved by using the proposed method over the general SVD-based solution found in Ref. 15.

V. Numerical Examples

In this section, test cases involving detailed thermal models of spacecraft in ongoing NASA missions are used to examine the accuracy of the algorithms presented in Secs. III and IV. These thermal models have been used extensively during the course of these missions. The termination criterion for both the proposed Gauss–Newton algorithm and the SQP method was set at 10^{-8}. This implies that numerical convergence is achieved when the Euclidean norm of the difference between two successive iterates is equal to or smaller than 10^{-8}.

In the first example, the proposed algorithms have been applied to a thermal model of Seawinds, a microwave radar instrument that orbits the Earth and measures near-surface wind speed and direction.[26] A schematic of the instrument is shown in Fig. 1. The thermal model consists of $N = 150$ internal nodes, $n = 91$ boundary nodes, 66 nonzero linear conduction coefficients, 15,392 nonzero radiation coefficients, and 8 heat sources. The set of observed nodes (the α set) consists of 19 nodes. The unobservable set (the β set) is formed by the remaining 47 nodes.

To generate artificial measurements, a random perturbation was applied to the boundary conditions. The solution for the α set of this perturbed thermal model played the role of the measured distribution; the solution for the β set of the perturbed model served as the true distribution, that is, the set of temperatures that have to be estimated as accurately as possible. The true temperature profile is plotted in Fig. 2a. The difference between the true and initially computed profiles is plotted in Fig. 2b. The mean value of the difference is 1.19 K.

At first it was assumed that there was no error in the measurements, that is, $\epsilon = 0$. The proposed Gauss–Newton algorithm for problem NP1 required only four iterations to converge. The error of the algorithm is plotted in Fig. 3a. The temperatures at the observed nodes were matched exactly, as expected. The average estimation error was 0.15 K, and the peak error was approximately 2.01 K. The standard SQP algorithm was also used; it required more than 40 iterations to converge. In terms of accuracy, the results of the two algorithms were almost identical. The error percentage of this method is shown in Fig. 3b. However, the CPU time required by the proposed algorithm was approximately 30 smaller than the CPU time for the SQP-based method.

Next, it was assumed that there was a random error in the measurements. The value of ϵ was set at $\epsilon = 7 \times 10^{-5}$, which is equivalent to

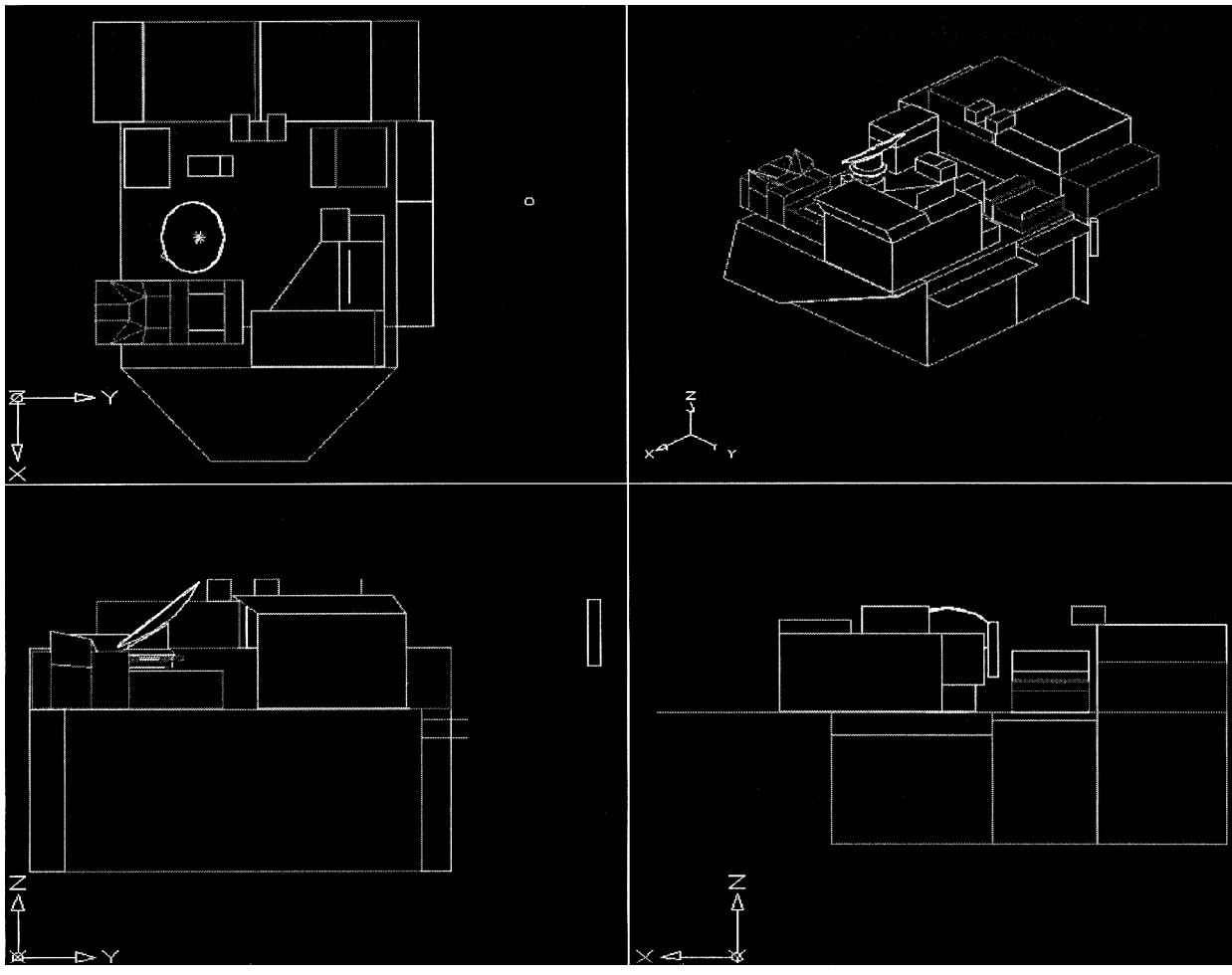

Fig. 1 Schematic of the Seawinds instrument from four different angles.

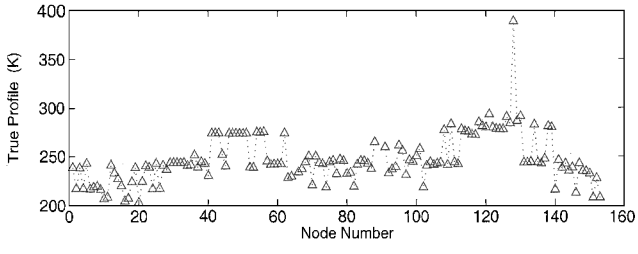

Fig. 2a True temperature distribution of Seawinds.

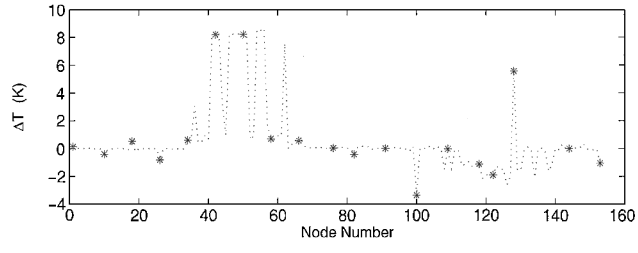

Fig. 2b Difference between true and initially computed distributions; observed nodes are shown with an asterisk.

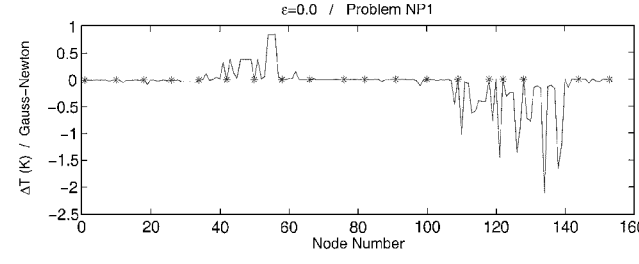

a) Proposed Gauss–Newton method

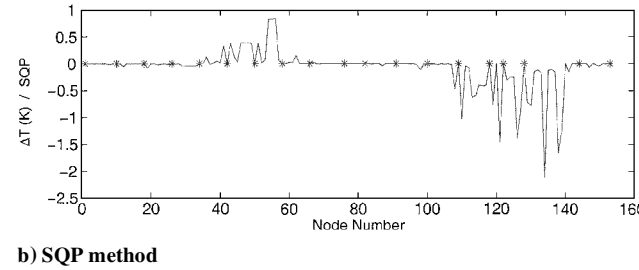

b) SQP method

Fig. 3 Error in the estimated temperatures via the NP1 formulation, tolerance $\epsilon = 0.0$; observed nodes shown with an asterisk.

an average measurement error of 2.27 K. The error of the proposed Gauss–Newton algorithm for problem NP1 is plotted in Fig. 4a, and the error of the equivalent SQP method is plotted in Fig. 4b. The proposed Gauss–Newton algorithm for required 5 iterations to compute the solution and it converged inside the feasibility region, and the SQP method required approximately 30 iterations and converged on the feasibility boundary. The proposed method was also more accurate than the SQP method. The maximum pointwise errors were 5.3 and 7.09 K, respectively, and the average errors were 0.74 and 0.99 K, respectively.

Analogous observations were made when the estimations for the β set were computed by solving the NP2 problem. For $\epsilon = 0$, both algorithms yielded identical results, but the proposed Gauss–Newton algorithm was much faster than the SQP method. The errors of both schemes for this case are shown in Fig. 5, the average error was 0.25 K. For $\epsilon = 7 \times 10^{-5}$, the results of the proposed algorithm

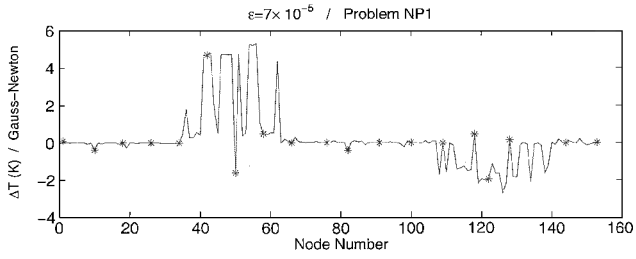

a) Proposed Gauss–Newton method

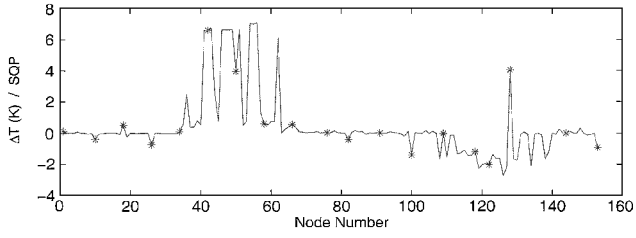

b) SQP method

Fig. 4 Error in the estimated temperatures via the NP1 formulation, tolerance $\epsilon = 7 \times 10^{-5}$; observed nodes shown with an asterisk.

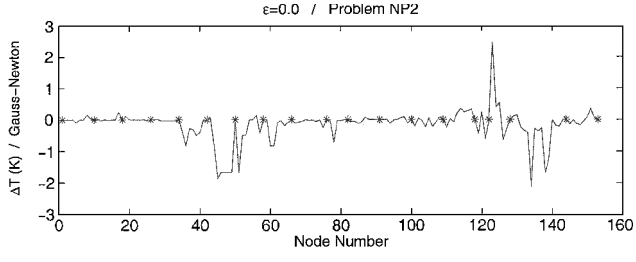

Proposed Gauss–Newton method

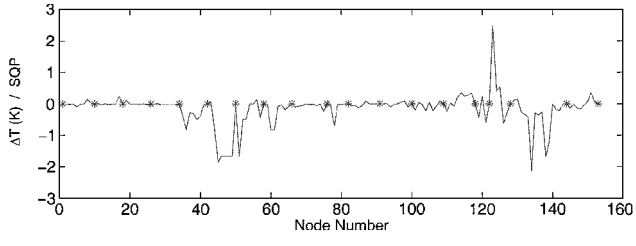

SQP method

Fig. 5 Error in the estimated temperatures via the NP2 formulation, tolerance $\epsilon = 0.0$; observed nodes shown with an asterisk.

were more accurate than those of the SQP method. The maximum pointwise errors were 2.45 and 5.82 K, respectively. The average errors were 0.22 and 0.85 K, respectively. The error plots for this test case are shown in Fig. 6.

In the second example, the proposed algorithms were applied to the thermal model of a proposed NASA flight experiment. This experiment was designed to demonstrate the feasibility of technology for large-size, segmented space telescopes. The primary mirror consists of three segments. Passive thermal control is provided by the sun shield, located in the back of the primary mirror. The thermal model of the spacecraft consists of $N = 1689$ interior nodes, $n = 30$ boundary nodes, 5153 nonzero conduction coefficients, and 100,417 nonzero radiation coefficients.

Two different boundary conditions were considered, a cold one and a hot one. For the purposes of the present study, the solution of the thermal model with the cold boundary conditions was considered to be the initially computed profile. A schematic of the thermal model, along with a plot of the cold solution is shown in Fig. 7. The measurements for the nodes of the α set, $\tilde{\boldsymbol{T}}$, were taken from the solution of the model with the hot boundary conditions, so that this (hot) solution could also serve as the true distribution for the β set. The initial profile and its difference from the true profile are plotted in Fig. 8. The average difference is 6.93 K, and the

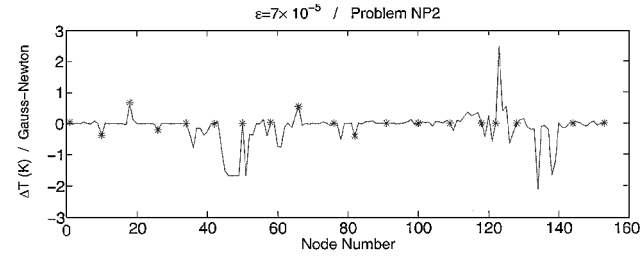

Proposed Gauss–Newton method

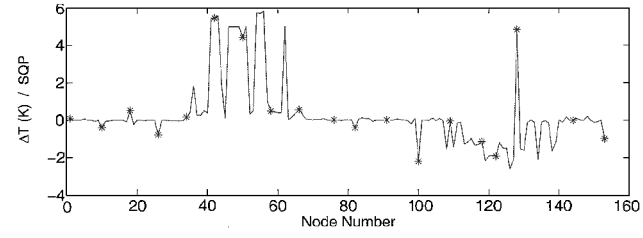

SQP method

Fig. 6 Error in the estimated temperatures via the NP2 formulation, tolerance $\epsilon = 7 \times 10^{-5}$; observed nodes shown with an asterisk.

maximum difference is 9.78 K. Such differences are not typically encountered in practice. They have been used in this study as a test of the robustness of the proposed algorithms.

Further, it was assumed that there were $M = 100$ available sensor locations. Sometimes various design considerations impose constraints on the possible location of the temperature sensors. In this example, it was assumed that there were no such restrictions. The metric of this problem was how well deformations are predicted on the primary mirror of the telescope given a global stiffness matrix coupled with a thermal model and measured temperature data. Consequently, the sensors were placed in the most important locations with respect to deformations of the primary mirror. For this purpose, the interior nodes of the system had to be ranked according to their effect on the deformations of interest. The ranking was performed via the following semi-empirical procedure.

Assume that there are M_1 nodes that influence the deformation on the primart mirror of the telescope. Under the assumption of linearity, the deformations $\boldsymbol{\xi}$ induced by temperature changes satisfy the following linear system:

$$K \cdot \boldsymbol{\xi} = W \cdot (\boldsymbol{T} - \boldsymbol{T}_0) \tag{83}$$

where K is the stiffness matrix of the structure, W is the temperature-to-stress transformation matrix, and $\boldsymbol{T}_0$ is the vector of the nominal, zeros-stress temperatures of the nodes of interest. The solution to Eq. (83) can be formally written as

$$\boldsymbol{\xi} = K^{\dagger} W \cdot (T - T_0) \tag{84}$$

where $K^{\dagger}$ is the pseudoinverse of K. Further, consider the submatrix consisting of the rows of the product $K^{\dagger}W$ that correspond to the elements of ξ that are interesting, and determine its singular values and singular vectors, e_i and $\boldsymbol{v}_i$, $i = 1, \ldots, M_1$, respectively, via the SVD. In general the SVD is not the most effective way to compute deformations. However, the problem of estimating the influence of each forcing term to the deformation vector is much harder than the problem of solving system (83), and the SVD can not be easily avoided in this case.

Once the singular values and vectors have been computed, the vector $\boldsymbol{V}$ defined as

$$\boldsymbol{V} = \sum_{i=1}^{m} e_i \cdot \boldsymbol{v}_i \tag{85}$$

is formed. Next, the elements of $\boldsymbol{V}$ are ranked according to their absolute values. This ranking gives a measure of the relative importance of the nodes of the system to the M_1 deformations of interest.

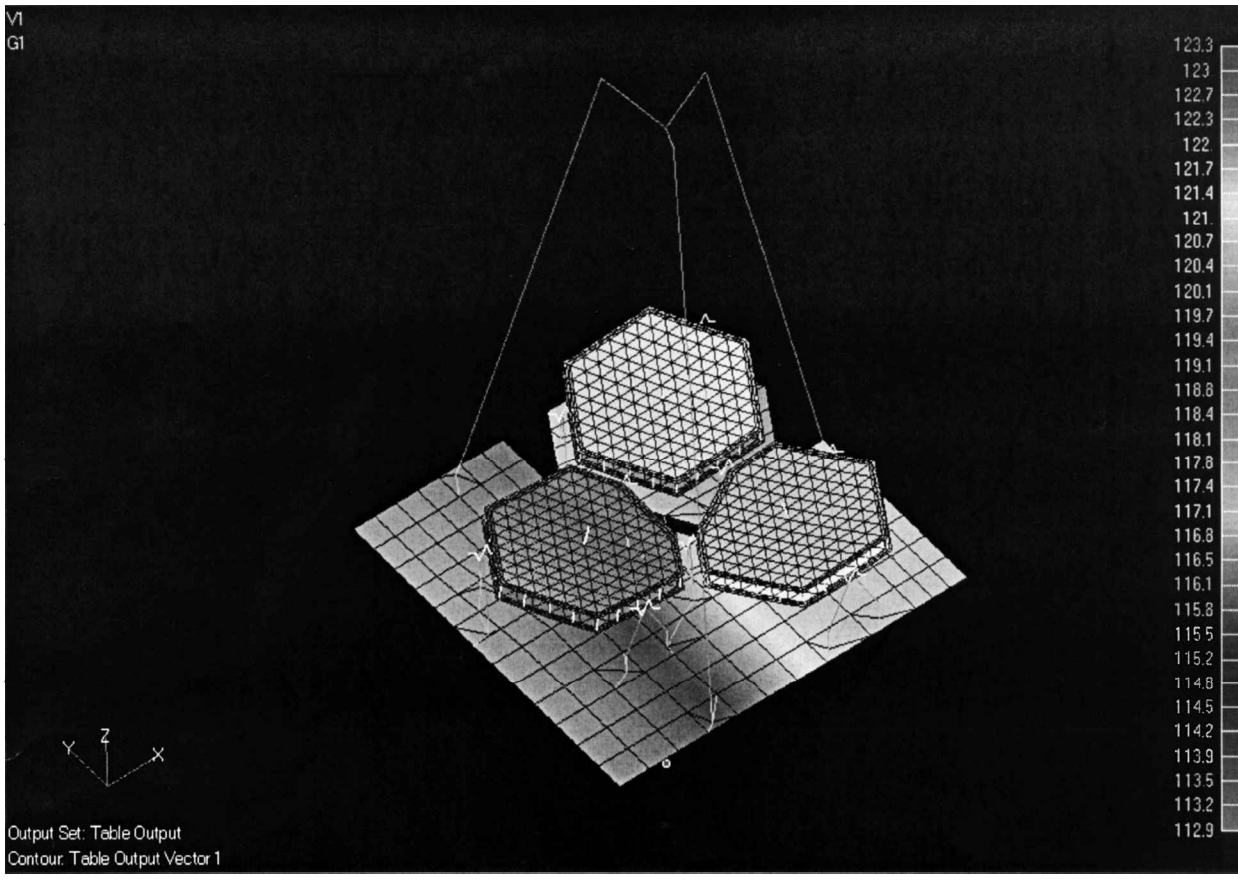

Fig. 7 Schematic of the spacecraft thermal model and initial temperatures.

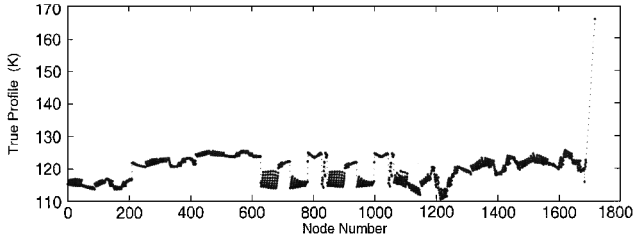

True temperature

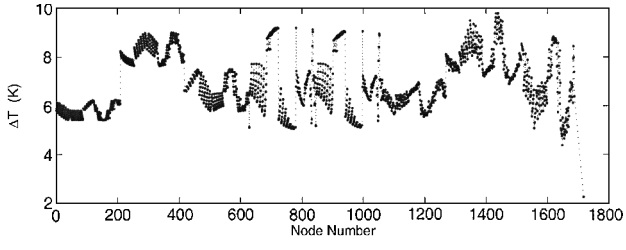

Difference between true and initial distributions

Fig. 8 Temperature distribution.

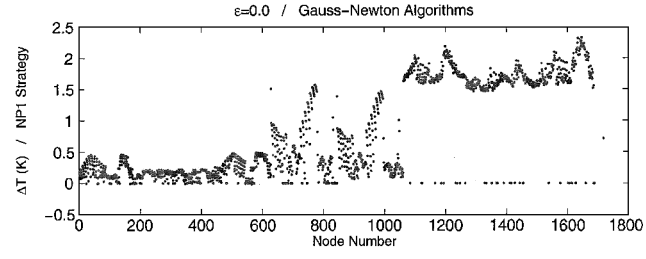

a) NP1 formulation

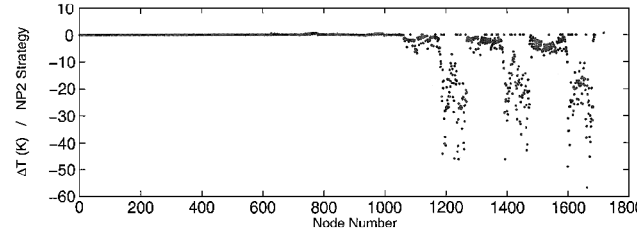

b) NP2 formulation

Fig. 9 Error of the proposed Gauss–Newton method in the estimated temperatures, tolerance $\epsilon = 0$.

In the present example, there are $M = 100$ observed nodes. The deformations of interest are the three translational displacements of each node in the model the primary mirror. The structural grid for the mirror consisted of 627 points. Therefore, the number of deformations of interest is $M_1 = 627 \times 3 = 1881$. The preceding semi-empirical procedure was employed for the determination of the observed nodes. Approximately one-third of them were located at the primary mirror, another third at the backplane of the primary mirror, and the other third at the supporting structure of the secondary mirror.

Next, the proposed Gauss–Newton algorithms were applied for the estimation of the temperature at the unobservable nodes. The estimation error via the NP1 formulation when $\epsilon = 0$ is shown in Fig. 9a. It can be verified that the algorithm produced satisfactory results; the average error was 0.8 K, and its maximum was less than 2.32 K (Recall that the average difference between true and computed profile was 6.93 K.) The test was repeated with the NP2 estimation strategy, but the results were not satisfactory. The error plot for the NP2 algorithm is given in Fig. 9b. It can be observed that the estimation errors were as high as 56.7 K, although their average was 3.89 K. For this test case, the equivalent SQP-based algorithm failed to converge, indicating that it is not as robust as the proposed Gauss–Newton method.

Subsequently, ϵ was set at 7×10^{-5}, which corresponds to an average measurement error of 1 K. The results were completely

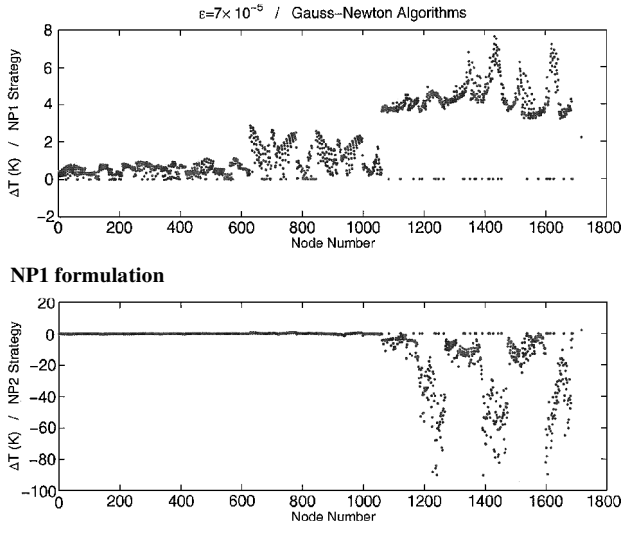

Fig. 10 Error of the proposed Gauss–Newton method in the estimated temperatures, tolerance $\epsilon = 7 \times 10^{-5}$.

analogous. The estimation errors are shown in Fig. 10. With the NP1 formulation, the average error was 2.5 K, and its maximum value was about 7.62 K. The algorithm based on the NP2 problem did not perform well and produced errors as high as 89.4 K (8.32 K on average). The equivalent SQP-based algorithm again failed to converge.

As already mentioned, the metric for this problem was the accuracy in the predictions for the deformations on the primary mirror. The difference between the initially computed thermal distribution and the true solution corresponds to deformations whose Euclidean norm is 55.56 μm. When $\epsilon = 0$, this norm was reduced to 5.62 μm with the NP1 solution, and 28.19 μm with the NP2 solution. In other words, there was a reduction by a factor of 10 and a factor of two, respectively. When $\epsilon = 7 \times 10^{-5}$, this norm was reduced to 14.24 μm with the NP1-based algorithm (reduction by a factor of four). On the other hand, the norm of the deformations predicted by the NP2-based algorithm remained practically unchanged, 55.95 μm, despite the large errors in the estimated temperatures.

To examine further the source of errors with the NP2 algorithm, we used the solution of the NP1 problem as the starting point for the NP2 algorithm. The algorithm converged to the same solution. In other words, the NP1 solution is suboptimal for the NP2 problem, but leads to a much more accurate estimate of both temperatures and deformations. The main difference between the two formulations is that an energy imbalance in the β set is permissible with the NP2 criterion. This imbalance undoubtedly leads to difficulties in this problem. An explanation for this is that, if the heat exchange between the α and β sets is poor, then temperatures can change significantly in the β set while still satisfying the measurement constraint. (Recall that the selection of the α set for this problem was based on the deformations on the primary mirror and not on the connectivity of the thermal model.) Hence, in this case, the NP2 criterion admits large temperature variations in the β set to reduce the cost. These temperature variations can get even larger in problems with significant measurement noise.

VI. Conclusions

Methods for estimating global temperatures from an a priori thermal model augmented with partially (and noisily) observed temperatures were developed. The mathematical formulation of this problem required nonlinear extensions and generalizations of analogous formulations that arise in structural analyses to determine global displacements from an a priori finite element model coupled with experimental test data that are restricted to a subset of the degrees of freedom of the system. After a number of considerations involving possible problem formulations, two strategies emerged for estimating the global temperature distribution. The first strategy minimizes the energy imbalance of the model at the observed nodes. The second strategy minimizes the energy imbalance over all of the nodes of the system. Knowledge of a subset of the temperature profile through (noisy) measurements is enforced as a quadratic constraint in both these problems. The problems defined by these two strategies were designated NP1 and NP2, respectively.

Solving the programming problems associated with NP1 and NP2 was a nontrivial problem in of itself. We discovered that state of the art off-the-shelf programs, such as SQP, were inadequate. In the telescope example we could never get SQP to converge. Alternative algorithms that exploit specific structure inherent in the network model and associated programming problems were developed. These algorithms converged on all of the problems, and in timing comparisons when SQP was successful, they ran typically 30 times faster than SQP.

A somewhat wide variation in performance of the methods was observed. On the moderately sized Seawinds problem, both NP1 and NP2 produced improvements over the initial model estimate, which does not incorporate temperature data. Furthermore, the improvements for the two methods were rather comparable. This contrasts with the results for the larger telescope model. The metric of this problem was how well deformations are predicted on the primary mirror of the telescope given a global stiffness matrix coupled with a thermal model and measured temperature data. The NP1 formulation yielded significant improvement over the predictions of the a priori model, but the results of the NP2 formulation were mixed: a moderate improvement if the measured temperatures were exact, and no improvement when there was a small error, 1 K, in the measurements. The disparity in these results suggests the underlying sensitivities in the solutions to the optimization criteria as a function of the thermal model and measurement locations. The lack of robustness with respect to the chosen criterion is indicative of difficulties in the problem formulation. This is underscored by the fact that the NP1 solution is suboptimal for the NP2 problem, but clearly leads to a much more accurate estimate of both temperatures and deformations. The variation in the solutions between NP1 and NP2 could serve as a diagnostic for the robustness of the thermal model and measurement set.

Acknowledgment

This work was prepared by the Jet Propulsion Laboratory, California Institute of Technology, under a contract with NASA.

References

[1]"Space Interferometry Mission," edited by R. Danner and S. Unwin, Jet Propulsion Lab., JPL Publ. 400-811, Pasadena, CA, 1999.

[2]"Next Generation Space Telescope," edited by H. S. Stockman, Association of Univs. for Research in Astronomy, Publ. STScI M9701, Baltimore, MD, 1997.

[3]Guyan, R. J., "Reduction of Stiffness and Mass Matrices," *AIAA Journal*, Vol. 3, No. 2, 1965, p. 370.

[4]Kidder, R. L., "Reduction of Structural Frequency Equations," *AIAA Journal*, Vol. 11, No. 6, 1973, p. 892.

[5]Levine, M. B., Milman, M. H., and Kissil, A., "Mode Shape Expansion Techniques for Prediciton: Experimental Evaluation," *AIAA Journal*, Vol. 34, No. 4, 1996, pp. 821–829.

[6]Kammer, D. C., "A Hybrid Approach to Test-Analysis Model Development for Large Space Structure," *Journal of Vibration and Acoustics*, Vol. 113, 1991, pp. 325–332.

[7]Smith, S. W., and Beattie, C. A., "Simultaneous Expansion and Orthogonalization of Measured Modes for Structure Identification," *Proceedings of AIAA Dynamics Specialist Conference*, AIAA, Washington, DC, 1990, pp. 261–270.

[8]Zimmerman, D. C., and Kaouk, M., "Structural Damage Detection Using a Subspace Rotation Algorithm," *Proceedings of the 33rd AIAA Structures, Structural Dynamics, and Materials Conference*, AIAA, Washington, DC, 1992, pp. 2341–2350.

[9]Beck, J. V., Blackwell, B., and St. Clair, C. R., Jr., *Inverse Heat Conduction*, Wiley Interscience, New York, 1985.

[10]Alifanov, O. M., *Inverse Heat Transfer Problems*, Springer-Verlag, Berlin, 1994.

[11]Hensel, E., *Inverse Theory and Applications*, Prentice–Hall, Englewood Cliffs, NJ, 1991.

[12]Kurpisz, K., and Nowak, A. J., *Inverse Thermal Problems*, Computational Mechanics, Southampton, England, U.K., 1995.

[13]Milman, M. H., and Petrick, W., "A Note on the Solution to a Common Thermal Network Problem Encountered in Heat Transfer Analysis of Spacecraft," *Applied Mathematical Modelling*, Vol. 24, 2000, pp. 861–879.

[14]Papalexandris, M. V., and Milman, M. H., "Active Control and Parameter Updating Techniques for Nonlinear Thermal Network Models," *Computational Mechanics*, Vol. 27, 2001, pp. 11–22.

[15]Golub, G., and Van Loan, C. F., *Matrix Computations*, Johns Hopkins Univ. Press, Baltimore, MD, 1983.

[16]Holman, J. P., *Heat Transfer*, 8th ed., McGraw–Hill, New York, 1997.

[17]Fletcher, R., *Practical Methods for Optimization*, 2nd ed., Wiley, New York, 1987.

[18]Gill, P. E., Murray, W., and Wright, M. H., *Practical Optimization*, Academic Press, San Diego, CA, 1981.

[19]Han, S. P., "A Globally Convergent Method for Nonlinear Programming," *Journal of Optimization Theory and Applications*, Vol. 22, No. 3, 1977, pp. 297–309.

[20]Powell, M. J. D., "Algorithm for Nonlinearly Constrained Optimization Calculations," *Numerical Analysis*, Vol. 630, Springer-Verlag, Berlin, 1978.

[21]Fletcher, R., "A Model Algorithm for Composite Nondifferentiable Optimization Problems," *Mathematical Programming Studies*, Vol. 17, 1982, pp. 67–76.

[22]Burke, J. V., and Han, S. P., "A Gauss–Newton Approach to Solving Generalized Inequalities," *Mathematics of Operations Research*, Vol. 11, No. 4, 1986, pp. 632–643.

[23]Sahba, M., "Globally Convergent Algorithm for Nonlinearly Constrained Optimization Problems," *Journal of Optimization Theory and Applications*, Vol. 52, No. 2, 1987, pp. 291–309.

[24]"MATLAB, Optimization Toolbox Manual," MathWorks, Natick, MA, 2000.

[25]Dennis, J. E., and Schnabel, R. B., *Numerical Methods for Unconstrained Optimization and Nonlinear Equations*, Society for Industrial and Applied Mathematics, Philadelphia, 1996.

[26]Seawinds, URL:http://winds.jpl.nasa.gov [cited 2001].

S. K. Aggarwal
Associate Editor